Thickness dependence of exchange coupling in epitaxial $Fe_3O_4/CoFe_2O_4$ soft/hard magnetic bilayers

G. Lavorato* and E. Winkler
Centro Atómico Bariloche, CNEA-CONICET, 8400 S.C. de Bariloche, Río Negro, Argentina

B. Rivas-Murias and F. Rivadulla
Center for Research in Biological Chemistry and Molecular Materials (CIQUS), University of Santiago de Compostela, 15782 Santiago de Compostela, Spain

(Received 29 March 2016; revised manuscript received 20 June 2016; published 1 August 2016)

Epitaxial magnetic heterostructures of (soft-)Fe_3O_4/(hard-)$CoFe_2O_4$ (001) have been fabricated with a varying thicknesses of soft ferrite from 5 to 25 nm. We report a change in the regime of magnetic interaction between the layers from rigid-coupling to exchange-spring behavior, above a critical thickness of the soft magnetic Fe_3O_4 layer. We show that the symmetry and epitaxial matching between the spinel structures of $CoFe_2O_4$ and Fe_3O_4 at the interface stabilize the Verwey transition close to the bulk value even for 5-nm-thick Fe_3O_4. The large interface exchange-coupling constant estimated from low-temperature $M(H)$ data confirmed the good quality of the ferrite-ferrite interface and the major role played by the interface in the magnetization dynamics. The results presented here constitute a model system for understanding the magnetic behavior of interfaces in core/shell nanoparticles and magnetic oxide-based spintronic devices.

DOI: 10.1103/PhysRevB.94.054405

I. INTRODUCTION

Exchange coupling in bimagnetic nanostructures has led to new applications [1–5] and new materials can be designed by changing the nature of each component [6], their relative size [7,8], or tuning the interface interactions [9,10]. For example, nanoparticles with core/shell structures have been synthesized seeking new permanent magnets [11,12], devices for high-density data storage [12], nanoheaters for hyperthermia [13], or image contrast agents [5]. At the same time, hard/soft bilayer thin films are of great interest for spin filtering and magnetic tunnel junctions [14,15]. In these systems the size of the soft phase determines the magnetization switching behavior and therefore the range of application of a particular system. In addition, it is known that magnetic bilayers present a critical thickness for the soft component below which both phases are rigidly exchange coupled and switch their magnetization simultaneously; whereas for larger thicknesses the soft phase nucleates and rotates reversibly at a lower magnetic field through an exchange-spring process. Despite the technological importance of this subject, most of the studies were focused on the magnetization reversal of metallic bilayers [16,17] and related features, such as training effects [18], whereas the mechanism that governs the reversal of the magnetization in soft-hard ferrite bilayers is still unclear [19–21].

In order to study the parameters that determine the transition from rigid coupling to exchange-spring behavior, we fabricated high-quality epitaxial heterostructures of soft/hard spinel oxides. We studied the structural relaxation and the magnetization reversal process as a function of the thickness of the soft phase. For the hard phase, insulating $CoFe_2O_4$ (CFO) was selected due to its high chemical stability and large magnetocrystalline anisotropy [22,23]. For the soft phase we selected Fe_3O_4. The main reasons are the chemical compatibility with CFO under typical pulsed laser deposition (PLD) conditions and the crystal symmetry matching with the cobalt ferrite spinel. Also, these nanostructures could serve as a model system to study the magnetic properties of hard-core/soft-shell nanoparticles where the shell thickness is more difficult to control precisely. In this context, the selection of Fe_3O_4 is interesting due to its increasing use in nanomedicine applications [24] or thermoelectrics [25,26]. Moreover, with this study we could also determine that the Verwey transition temperature T_V of Fe_3O_4 thin films is stabilized by the presence of a CFO underlayer, apparently due to the crystal symmetry matching and the good interface quality.

II. EXPERIMENTAL DETAILS

A series of Fe_3O_4/CFO spinel bilayers were grown by PLD (KrF laser, $\lambda = 248$ nm) on $MgAl_2O_4$ (MAO) (001) spinel substrates (CrysTec, $a_S = 0.8083$ nm) where the soft Fe_3O_4 thickness was varied from 0 to 25 nm keeping the hard CFO layer thickness fixed at 25 nm. A $CoFe_2O_4$ target was prepared by a solid-state reaction of Fe and Co (99.9% purity) powders sintered at 1400 °C after intermediate grinding steps, and a Fe_3O_4 target was prepared according to the procedure described in Ref. [27]. During the CFO deposition the substrate temperature was set to 640 °C, the oxygen pressure was kept at 10^{-3} Torr, and the deposition rate was fixed at 0.7 nm/min by employing a laser fluence of 1.4 J/cm^2. For the Fe_3O_4 film deposition the substrate temperature was set to 500 °C, the oxygen pressure was kept at 10^{-7} Torr, and the deposition rate was at 2.0 nm/min by using a laser fluence of 3.0 J/cm^2. X-ray analyses were performed in a Panalytical X'Pert Pro diffractometer with Cu $K\alpha$ radiation. A superconducting quantum interference device magnetometer (Quantum Design, maximum field of ±50 kOe) was used to study the field and temperature dependence of the magnetization. The measurements were conducted by applying the magnetic field on the plane of the film along the [100] direction, and magnetization versus temperature measurements were performed through the zero-field-cooled protocol with an applied field of 500 Oe. The

*Corresponding author: lavorato@cab.cnea.gov.ar

diamagnetic contribution of the substrate was subtracted from the data presented in the paper.

III. RESULTS AND DISCUSSION

A. Film deposition and structural relaxation

The study of the thickness dependence of the magnetic properties depends on the fabrication of good-quality thin films, and many different approaches have been performed for pulsed-laser deposition of spinel ferrites [28–30]. In our case, regarding the deposition of the CFO layer, we found that different conditions (including higher oxygen pressure and higher laser fluence) lead to films with a lower degree of epitaxy, probably due to different growth modes [31]. We also found that a high-quality Fe_3O_4 layer requires a very low base pressure and an accurate control of the deposition rate in order to retain a good stoichiometry. The Verwey transition is known to be very sensitive to the stoichiometry of the film [32], so the observation of a high T_V (as will be discussed later) is an indication of a good-quality Fe_3O_4 layer.

X-ray diffraction (XRD) θ-2θ scans are shown in Fig. 1. Only the (00ℓ) peaks from the substrate, CFO, and Fe_3O_4 were observed in full length scans, confirming the deposition of c-axis-oriented single phases. Detailed scans around the (004) spinel reflection are shown in Fig. 1(b). The Laue oscillations observed for the isolated CFO film indicate a long-range coherence length $l_c = 2\pi/\Delta q \sim 23.7$ nm (where

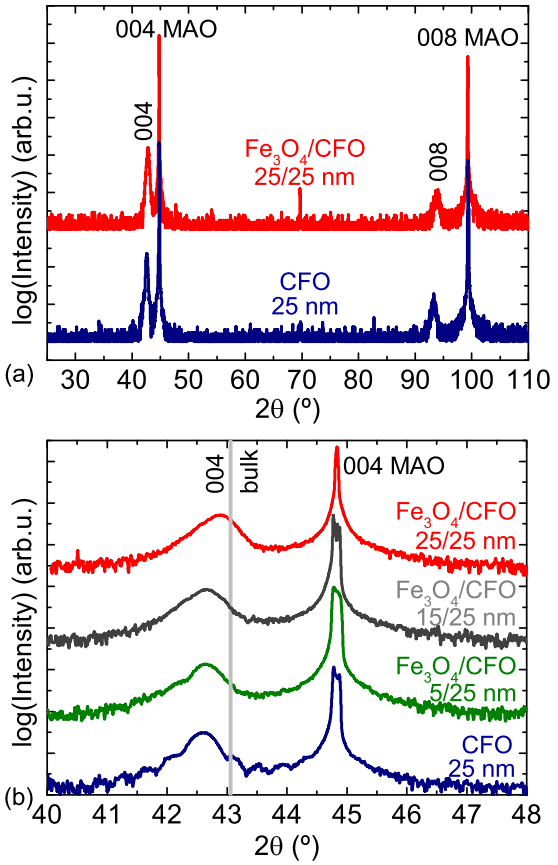

FIG. 1. (a) Full-length and (b) detailed θ-2θ XRD scans of Fe_3O_4/CFO bilayers and isolated CFO films.

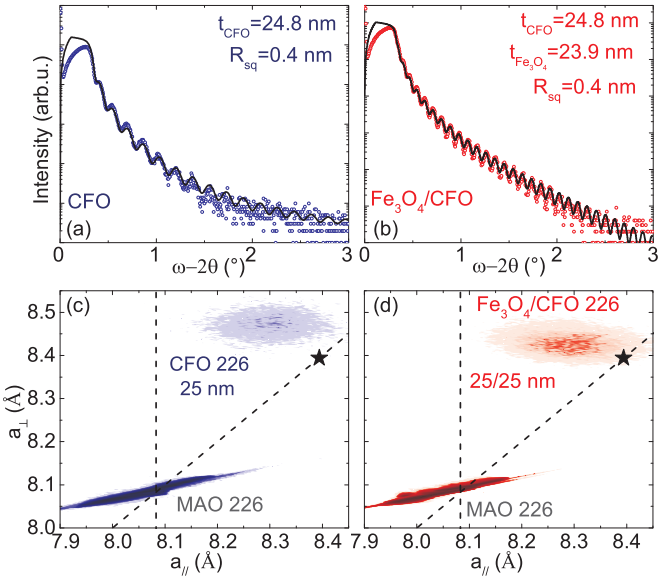

FIG. 2. (a) and (b) XRR and (c) and (d) RSM scans of isolated CFO films and Fe_3O_4/CFO (25/25)-nm bilayers. Solid lines indicate XRR fits, dashed lines indicate $R = 0$ and $R = 1$, and a star indicates the lattice parameter for bulk CFO and Fe_3O_4.

$q = 4\pi sen(\theta)/\lambda$ is the scattering vector) that is very close to the whole thickness of the film determined by x-ray reflectivity (XRR) [Fig. 2(a)], showing a good crystalline coherence [33]. In the case of the bilayers, only a single (004) reflection is observed due to the similarity between the lattice parameters of $a_{CFO} = 0.8392$ and $a_{Fe_3O_4} = 0.8396$ nm.

High-resolution reciprocal space maps (RSMs) around the asymmetric (226) spinel reflection are shown in Figs. 2(c) and 2(d). As substrate and film have the same spinel structure, RSMs are represented in lattice parameter units. From these data, the perpendicular $a_\perp$ and the in-plane $a_\parallel$ lattice parameters for the films were estimated (see Fig. 3). However, the almost identical lattice parameters of CFO and Fe_3O_4 spinels makes it impossible to distinguish between them, and therefore an average value was obtained from the RSM plots. The perpendicular strain $\epsilon_\perp = (a_\perp - a_L)/a_L$, the in-plane strain $\epsilon_\parallel = (a_\parallel - a_L)/a_L$, and the relaxation parameter

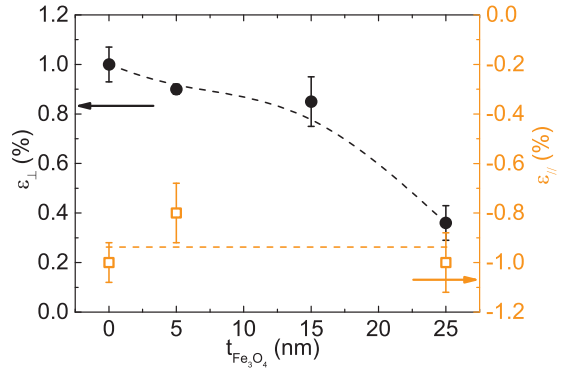

FIG. 3. Fe_3O_4 thickness dependence of in-plane (empty squares) and perpendicular strains (full circles) estimated from RSM and XRD patterns (lines are guides to the eye).

$R = (a_{\parallel} - a_S)/(a_L - a_S)$ were computed from these data, where a_S and a_L represent the lattice parameters of the substrate and the film, respectively (for the bilayers we used an average of $a_L = 0.8394$ nm).

The structural analysis shows that the films are compressed in plane and tensile-strained along the perpendicular direction although partially relaxed. The relaxation parameter $R \sim 73\%$ for the isolated CFO layer is in agreement with previous reports on Fe_3O_4/MAO where a critical relaxation thickness around 5 nm was identified [34]. Given the structural similarities between Fe_3O_4 and CFO, a similar relaxation pathway can be expected for both spinels. The Poisson ratio (ν), calculated from the relationship between $\epsilon_{\perp}$ and $\epsilon_{\parallel}$ according to $\epsilon_{\perp} = \epsilon_{\parallel}(-2\nu)/(1-\nu)$ [35], is $\sim 0.31(2)$ for every thickness, except for the 25-nm-Fe_3O_4/25-nm-CFO, where $\nu \sim 0.15$. These values are close to $\nu \sim 0.2$ and $\nu \sim 0.13$, reported for CFO and Fe_3O_4, respectively, on MAO [36–38]. Small deviations may be the result of inhomogeneous strain in partially relaxed films, which make the comparison with bulk values of ν difficult.

B. Magnetic properties

The strain is expected to play a major role in determining the magnetic anisotropy due to the large magnetostriction of CFO. Fritsch and Ederer calculated the effect of epitaxial strain on the magnetocrystalline anisotropy of CFO and concluded that compressive strain favors in-plane orientation of the magnetization [36]. The magnetoelastic anisotropy energy (associated with an uniaxial anisotropy due to the tetragonal distortion) is given by $K_{ME} = \frac{3}{2}\lambda_{100}(c_{11} - c_{12})(\epsilon_{\perp} - \epsilon_{\parallel})$ where $c_{11} = 2.73 \times 10^{12}$, $c_{12} = 1.06 \times 10^{12}$ erg/cm^3, and $\lambda_{100} = -590 \times 10^{-6}$ denote the bulk CFO elastic constants and magnetostriction, respectively [22,39]. On the other hand, the cubic magnetocrystalline anisotropy energy is given by $K_{MC} = K_1/4$, where K_1 is the low-temperature magnetocrystalline anisotropy constant of CFO [40]. In our 25-nm-thick CFO layer, K_{ME} and K_{MC} were estimated at $\sim -2 \times 10^7$ and 5×10^6 erg/cm^3, respectively; the negative sign of K_{ME} indicates that a hard axis perpendicular to the plane is promoted, leading to biaxial in-plane anisotropy. It is also worth noting that K_{ME} is larger than K_{MC}, favoring in-plane orientation of the magnetization. This is further favored by the shape magnetostatic anisotropy $K_{MS} = -2\pi M_S^2 \sim -1 \times 10^6$ erg/cm^3.

A comparison of the in-plane and out-of-plane hysteresis loops (Fig. 4) confirms the above calculation. All the films show an out-of-plane hard axis ([001] direction), whereas higher coercivity and slightly larger magnetization, compatible with an easy direction for the magnetization, are observed in-plane. No differences were found between [100] and [010] directions, which is consistent with a biaxial compressive strain produced by cubic MAO. The in-plane biaxial anisotropy is preserved for all the bilayers, irrespective of their total thicknesses. On the other hand, and in agreement with previous reports [15,41,42], we observed a low-field magnetization contraction in the in-plane hysteresis loop of CFO. This is shown in Fig. 4(a) for a 25-nm-thick film of CFO ($t_{Fe_3O_4} = 0$ nm). Such an anomaly can be explained by the contributions of a surface anisotropy, different from the bulk due to the broken symmetry at the surface of the film. In support

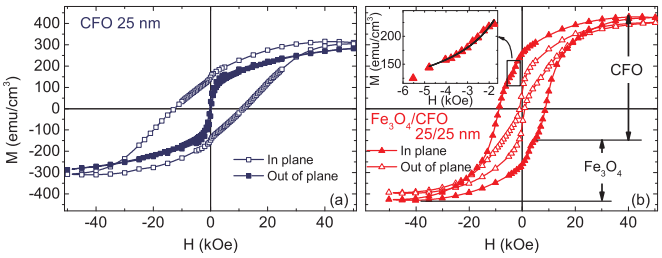

FIG. 4. In-plane and out-of-plane hysteresis loops of (a) isolated CFO films and (b) Fe_3O_4/CFO (25/25)-nm bilayers measured at 10 K. The inset shows the fitting of part of the curve according to the $1/\sqrt{H}$ dependence expected for exchange-spring magnets.

of this hypothesis, we observed that this anomaly is suppressed when growing a Fe_3O_4 layer on top of the CFO film. We can hypothesize that the magnetite is stabilizing the surface of CFO by increasing the effective coordination number of the surface magnetic ions due to the exchange coupling at the interface and their crystal symmetry matching [43].

The saturation magnetization of our bilayers [shown in Fig. 4(a)] is found to be reduced compared with bulk materials (480 emu/cm^3 for CFO) as is usually observed in thin films due to surface spin disorder [44]. When Fe_3O_4 is grown on top of the CFO layer, the surface disorder of CFO is reduced, and its magnetic moment is stabilized. This fact can explain the magnetization ratio of both layers in (25/25)-nm films as highlighted in Fig. 4(b). In addition,the remanence and coercivity (H_C) of the Fe_3O_4/CFO bilayers are increased for the thinnest Fe_3O_4, indicating that the interface is playing a major role in the overall magnetization process. In fact, as is revealed in Fig. 5(a), the H_C results 13.1 and 16.5 kOe for CFO and (5/25)-nm Fe_3O_4/CFO, respectively. For thicker Fe_3O_4 layers, the coercivity is reduced ($H_C \sim 12.9$ and 8.7 kOe for (15/25)- and (25/25)-nm Fe_3O_4/CFO bilayers, respectively), indicating that the switching field of the hard layer is lowered by the exchange coupling with the soft layer as we will analyze below.

The crystal symmetry matching also helps stabilizing the Verwey transition in ultrathin layers of Fe_3O_4. In magnetite thin films, a reduction or suppression of T_V is usually observed when decreasing the film thickness due to nonstoichiometry and to the increase in the density of antiphase boundaries [44,45], originated by partial dislocations due to lattice [32] or symmetry mismatch [34]. In Fig. 6 we show the temperature dependence of the magnetization of Fe_3O_4/CFO bilayers. Surprisingly, the Verwey transition, determined from the maximum of dM/dT, is very close to the bulk value of $T_V \sim 125$ K, even for $t_{Fe_3O_4} = 5$ nm. Although our preliminary results do not let us unambiguously explain the origin of the high T_V, we think that the underlayer of CFO may be responsible for this effect. Unlike Fe_3O_4 films grown on MgO, the spinel structure of the CFO layer could disfavor the formation of antiphase boundaries by crystal symmetry matching. At the same time, the lattice mismatch is reduced below -1.0% compared to Fe_3O_4 grown on MAO (-3.8%) or $SrTiO_3$ (-7.5%). Both conditions could be promoting the growth of larger domain sizes and a high T_V even for 5-nm Fe_3O_4 films. However,

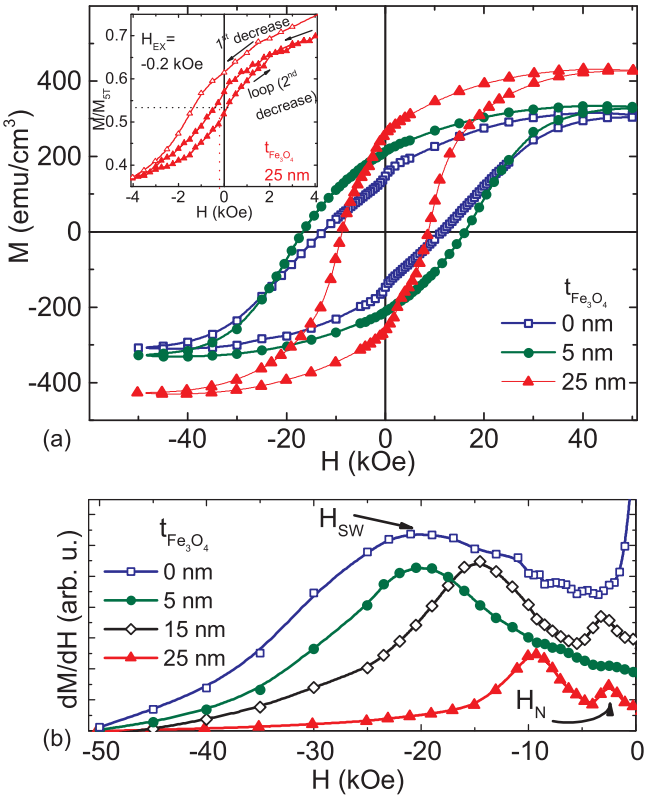

FIG. 5. (a) In-plane hysteresis loops and (b) dM/dH curves (where the maxima indicate the reversion fields) of isolated CFO films and Fe_3O_4/CFO bilayers for different Fe_3O_4 thicknesses measured at 10 K. (c) Exchange-biased soft layer loop of Fe_3O_4/CFO 25/25 nm measured from −4 kOe after decreasing the field from +50 kOe.

further experimental work is needed to corroborate these hypotheses.

Once the high quality of the interface between Fe_3O_4 and CFO has been established, we turn our attention to the magnetization reversal process in Fe_3O_4/CFO bilayers. The main results are summarized in Fig. 5. The loops for 15- and 25-nm-Fe_3O_4/25-nm-CFO layers display two switching

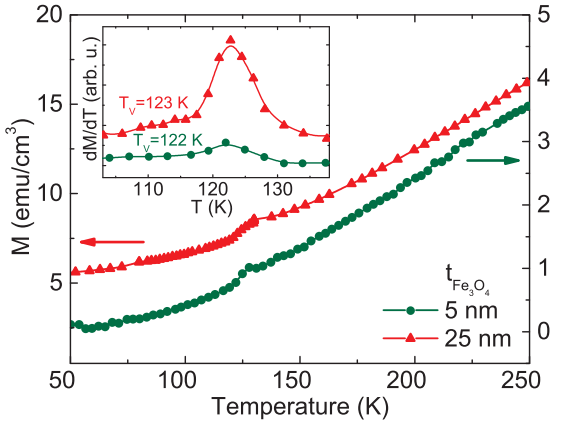

FIG. 6. Temperature dependence of magnetization and dM/dT (inset) indicating the Verwey transition temperature of Fe_3O_4/CFO (25/25)- and (5/25)-nm bilayers.

events as expected for partially decoupled magnetic layers. From the maxima of the derivative of $M(H)$ [Fig. 5(b)], the reversal fields were obtained: the high-field maximum was identified as the irreversible switching field of the hard-phase (H_{SW}) whereas the lowest reversal field was associated with the nucleation field of the soft-phase (H_N). In addition, the shape of the hysteresis curve of (25/25)-nm bilayers suggests an exchange-spring reversal process where the magnetization does not saturate after the soft-phase reversal, following a $1/\sqrt{H}$ dependence [46]. Assuming this situation, part of the magnetization curve [shown in Fig. 4(b)] was fitted with $M = 2M_S(\sqrt{H_B/H} - 1)$, where M_S is the magnetization of the soft phase and H_B is a parameter called the bending field. From the fit, a $M_S \sim 180$ emu/cm^3 and a $H_B \sim 2480$ Oe were obtained, the latter in agreement with H_N highlighted in Fig. 5(b).

According to the exchange-spring theory for hard/soft bilayers [16,47], the individual/coupled reversal of both layers is governed by the relative magnitudes of the soft layer thickness t_S and the exchange length of the hard layer l_{eH}. For $t_S < l_{eH}$, simultaneous switching of both phases occurs at a switching field $H_{SW} = 2\frac{K_H t_H + K_S t_S}{M_H t_H + M_S t_S}$. In this case M and K correspond to the saturation magnetization and magnetic anisotropy, and the suffixes S and H stand for the soft and hard phases, respectively. For $t_S > l_{eH}$, the soft and hard phases will reverse at different fields, and a characteristic two-phase magnetization loop will be observed. If $K_H > K_S$ is assumed, the nucleation field of the soft layer can be described by $H_N = \frac{\pi^2 A_S}{2M_S t_S^2}$, where A_S represents the exchange stiffness of the soft layer. The switching and nucleation fields obtained from our data and the calculated values (considering $K_H \sim 5 \times 10^6$ erg/cm^3, $A_S \sim 7 \times 10^{-7}$ erg/cm, and bulk $M_H \sim 480$ and $M_S \sim 510$ emu/cm^3 [40]) are shown in Fig. 7(a). It can be seen that our data are well reproduced by the theory, and a critical thickness $t_C \sim 8$ nm, defined as the maximum soft layer thickness for rigid coupling, can be estimated. This value is in very good agreement with the calculated exchange length of the hard layer given by $l_{eH} = (\frac{A_H}{2\pi M_H^2})^{1/2} = 8.3$ nm, where $A_H \sim 1 \times 10^{-6}$ erg/cm [40].

Notice that the overall magnetization reversal process can be accounted for by the exchange-spring theory which considers a perfectly rigid hard layer coupled to a zero-

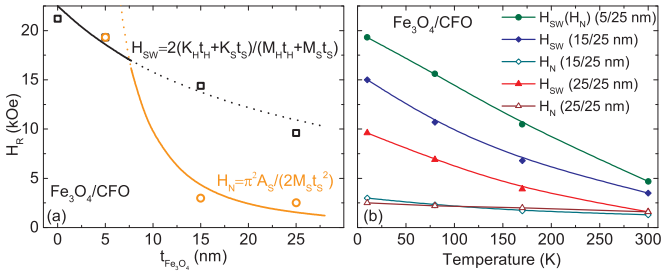

FIG. 7. Dependence of the switching field (H_{SW}) of the hard phase and the nucleation field (H_N) of the soft phase as a function of (a) the Fe_3O_4 film thickness and (b) the temperature. The lines in (a) indicate the fitting according to the corresponding equations. The lines in (b) serve as a guide to the eye.

anisotropy soft layer [48]. As we have seen, within this model H_N is determined by the exchange field of the soft phase, which should be fully reversible for $H < H_{SW}$ [16,46]. However, the minor loop shown in the inset of Fig. 5(a) evidences a greater complexity of the real system. This measurement was performed by saturating the sample in a +50-kOe field and applying then a reverse field down to −4 kOe. The hysteresis curve of the soft layer (minor loop of the bilayer) was subsequently recorded between −4 and +4 kOe. The differences between the first and the second decreases in the minor loop can be attributed to a partial irreversible rotation of the CFO layer due to the wide H_{SW} distribution [49], whereas the presence of a non-null coercive field is due to the finite anisotropy of the Fe_3O_4 phase. The strength of the exchange interaction can be estimated by the exchange bias field of the minor loop $H_{EX} = J_{EX}/M_S t_S$ [17,50] which results in −0.2 kOe. At the same time, the exchange stiffness constant at the interface can be inferred from $J_{EX} \sim A_{EX}/a_L$, and the estimated $A_{EX} \sim 1 \times 10^{-7}$-erg/cm value is close to the exchange stiffness of Fe_3O_4, indicating a good structural and magnetic quality of the interface.

Our study follows with the analysis of the temperature variation of H_{SW} and H_N up to 300 K, shown in Fig. 7(b). The rigid-coupling regime is preserved in the whole temperature range for (5/25)-nm Fe_3O_4/CFO bilayers, where H_{SW} at 300 K is four times lower than the low-temperature value. A similar reduction is observed for the switching fields of bilayers with higher Fe_3O_4 thicknesses. Two distinct reversal fields are observed for (15/25)- and (25/25)-nm bilayers in the whole temperature range, and their nucleation fields at 300 K decrease between 2 and 1.5 times, respectively, when compared with the low-temperature values. In every case, H_{SW} decreases faster than H_N because the former is ruled by the temperature dependence of the anisotropy of the hard phase, whereas the latter is determined by the magnetization and exchange stiffness of the soft phase, which are much less temperature dependent.

IV. CONCLUSIONS

A critical thickness for the rigid-coupling regime was experimentally identified in epitaxial $Fe_3O_4/CoFe_2O_4$ bilayers deposited on $MgAl_2O_4$ (001) by pulsed laser deposition. Our results indicate that the bilayers behave as rigidly coupled magnets for Fe_3O_4 thicknesses lower than 8 nm and as exchange-spring magnets for thicker Fe_3O_4 layers. Crystal symmetry matching at the interface stabilizes the Verwey transition in ultrathin layers of Fe_3O_4 and leads to a large interface exchange-coupling constant that governs the magnetization dynamics of the bilayers. Our results are useful as a model to interpret the behavior of interfaces in core/shell bimagnetic nanoparticles and oxide magnetoresistive systems.

ACKNOWLEDGMENTS

F.R. wants to acknowledge financial support from the MINECO-Spain (Project No. MAT2013-44673-R). B.R.-M. acknowledges support from Xunta de Galicia (Project No. EM2013/038). G.L. acknowledges the Bec. Ar Program for financial support. G.L. and E.W. thank ANPCyT through Grant No. PICT-2012-0492 and UNCuyo through Grant No. C011.

[1] H. Zeng, J. Li, J. P. Liu, Z. L. Wang, and S. Sun, Nature (London) **420**, 395 (2002).
[2] V. Skumryev, S. Stoyanov, Y. Zhang, G. Hadjipanayis, D. Givord, and J. Nogues, Nature (London) **423**, 850 (2003).
[3] J. Nogués, J. Sort, V. Langlais, V. Skumryev, S. Surinach, J. Munoz, and M. Baró, Phys. Rep. **422**, 65 (2005).
[4] R. Ramesh and N. A. Spaldin, Nat. Mater. **6**, 21 (2007).
[5] A. López-Ortega, M. Estrader, G. Salazar-Alvarez, A. G. Roca, and J. Nogués, Phys. Rep. **553**, 1 (2015).
[6] E. L. Winkler, E. Lima, D. Tobia, M. E. Saleta, H. E. Troiani, E. Agostinelli, D. Fiorani, and R. D. Zysler, Appl. Phys. Lett. **101**, 252405 (2012).
[7] A. López-Ortega, M. Estrader, G. Salazar-Alvarez, S. Estradé, I. V. Golosovsky, R. K. Dumas, D. J. Keavney, M. Vasilakaki, K. N. Trohidou, J. Sort *et al.*, Nanoscale **4**, 5138 (2012).
[8] G. C. Lavorato, E. Lima, Jr., D. Tobia, D. Fiorani, H. E. Troiani, R. D. Zysler, and E. L. Winkler, Nanotechnology **25**, 355704 (2014).
[9] M. Estrader, A. López-Ortega, S. Estradé, I. V. Golosovsky, G. Salazar-Alvarez, M. Vasilakaki, K. N. Trohidou, M. Varela, D. C. Stanley, M. Sinko, M. J. Pechan, D. J. Keavney, F. Peiró, S. Suriñach, M. D. Baró, and J. Nogués, Nat. Commun. **4**, 2960 (2013).
[10] G. C. Lavorato, D. Peddis, E. Lima, H. E. Troiani, E. Agostinelli, D. Fiorani, R. D. Zysler, and E. L. Winkler, J. Phys. Chem. C **119**, 15755 (2015).
[11] F. Liu, J. Zhu, W. Yang, Y. Dong, Y. Hou, C. Zhang, H. Yin, and S. Sun, Angew. Chem., Int. Ed. **53**, 2176 (2014).
[12] D. J. Sellmyer, B. Balamurugan, B. Das, P. Mukherjee, R. Skomski, and G. Hadjipanayis, J. Appl. Phys. **117**, 172609 (2015).
[13] J. Lee, J. Jang, J. Choi, S. Moon, S. Noh, J. Kim, J. Kim, I. Kim, K. Park, and J. Cheon, Nat. Nanotechnol. **6**, 418 (2011).
[14] U. Lüders, A. Barthélémy, M. Bibes, K. Bouzehouane, S. Fusil, E. Jacquet, J.-P. Contour, J.-F. Bobo, J. Fontcuberta, and A. Fert, Adv. Mater. **18**, 1733 (2006).
[15] A. V. Ramos, J.-B. Moussy, M.-J. Guittet, M. Gautier-Soyer, C. Gatel, P. Bayle-Guillemaud, B. Warot-Fonrose, and E. Snoeck, Phys. Rev. B **75**, 224421 (2007).
[16] E. E. Fullerton, J. S. Jiang, and S. D. Bader, J. Magn. Magn. Mater. **200**, 392 (1999).
[17] J. Y. Gu, J. Burgess, and C.-Y. You, J. Appl. Phys. **107**, 103918 (2010).
[18] C. Binek, S. Polisetty, X. He, and A. Berger, Phys. Rev. Lett. **96**, 067201 (2006).

[19] Y. Suzuki, R. B. van Dover, E. M. Gyorgy, J. M. Phillips, and R. J. Felder, Phys. Rev. B **53**, 14016 (1996).
[20] M. G. Chapline and S. X. Wang, J. Appl. Phys. **97**, 123901 (2005).
[21] C. A. Kleint, M. K. Krause, R. Höhne, T. Walter, H. C. Semmelhack, M. Lorenz, and P. Esquinazi, J. Appl. Phys. **84**, 5097 (1998).
[22] R. Bozorth, E. F. Tilden, and A. J. Williams, Phys. Rev. **99**, 1788 (1955).
[23] A. V. Ramos, M.-J. Guittet, J.-B. Moussy, R. Mattana, C. Deranlot, F. Petroff, and C. Gatel, Appl. Phys. Lett. **91**, 122107 (2007).
[24] Q. A. Pankhurst, N. T. K. Thanh, S. K. Jones, and J. Dobson, J. Phys. D. Appl. Phys. **42**, 224001 (2009).
[25] N.-W. Park, W.-Y. Lee, J.-A. Kim, K. Song, H. Lim, W.-D. Kim, S.-G. Yoon, and S.-K. Lee, Nanoscale Res. Lett. **9**, 96 (2014).
[26] R. Ramos, T. Kikkawa, K. Uchida, H. Adachi, I. Lucas, M. H. Aguirre, P. Algarabel, L. Morellón, S. Maekawa, E. Saitoh, and M. R. Ibarra, Appl. Phys. Lett. **102**, 072413 (2013).
[27] J. M. De Teresa, A. Fernández-Pacheco, L. Morellon, J. Orna, J. A. Pardo, D. Serrate, P. A. Algarabel, and M. R. Ibarra, Microelectron. Eng. **84**, 1660 (2007).
[28] G. Hu, J. H. Choi, C. B. Eom, V. G. Harris, and Y. Suzuki, Phys. Rev. B **62**, R779(R) (2000).
[29] J. H. Yin, J. Ding, B. H. Liu, J. B. Yi, X. S. Miao, and J. S. Chen, J. Appl. Phys. **101**, 09K509 (2007).
[30] J. X. Ma, D. Mazumdar, G. Kim, H. Sato, N. Z. Bao, and A. Gupta, J. Appl. Phys. **108**, 063917 (2010).
[31] J. A. Moyer, R. Gao, P. Schiffer, and L. W. Martin, Sci. Rep. **5**, 10363 (2015).
[32] X. H. Liu, A. D. Rata, C. F. Chang, A. C. Komarek, and L. H. Tjeng, Phys. Rev. B **90**, 125142 (2014).
[33] M. Birkholz, *Thin Films Analysis by X-Ray Scattering* (Wiley-VCH, Weinheim, 2006).
[34] M. Luysberg, R. G. S. Sofin, S. K. Arora, and I. V. Shvets, Phys. Rev. B **80**, 024111 (2009).
[35] J. Y. Tsao, *Materials Fundamentals of Molecular Beam Epitaxy* (Academic, San Diego, 2012).
[36] D. Fritsch and C. Ederer, Phys. Rev. B **82**, 104117 (2010).
[37] M. Foerster, M. Iliev, N. Dix, X. Martí, M. Barchuk, F. Sínchez, and J. Fontcuberta, Adv. Funct. Mater. **22**, 4344 (2012).
[38] M. Ziese, arXiv:1103.3666.
[39] A. Lisfi, C. M. Williams, L. T. Nguyen, J. C. Lodder, A. Coleman, H. Corcoran, A. Johnson, P. Chang, A. Kumar, and W. Morgan, Phys. Rev. B **76**, 054405 (2007).
[40] J. M. Coey, *Magnetism and Magnetic Materials* (Cambridge University Press, Cambridge, U.K., 2010).
[41] L. Horng, G. Chern, M. Chen, P. Kang, and D. Lee, J. Magn. Magn. Mater. **270**, 389 (2004).
[42] F. Rigato, J. Geshev, V. Skumryev, and J. Fontcuberta, J. Appl. Phys. **106**, 113924 (2009).
[43] R. H. Kodama, A. E. Berkowitz, E. J. McNiff, Jr., and S. Foner, Phys. Rev. Lett. **77**, 394 (1996).
[44] J. Orna, P. A. Algarabel, L. Morellón, J. A. Pardo, J. M. de Teresa, R. López Antón, F. Bartolomé, L. M. García, J. Bartolomé, J. C. Cezar, and A. Wildes, Phys. Rev. B **81**, 144420 (2010).
[45] W. Eerenstein, T. T. M. Palstra, T. Hibma, and S. Celotto, Phys. Rev. B **66**, 201101(R) (2002).
[46] Y. Wang, X. He, T. Mukherjee, M. Fitzsimmons, S. Sahoo, and C. Binek, J. Appl. Phys. **110**, 103914 (2011).
[47] S.-s. Yan, J. A. Barnard, F.-t. Xu, J. L. Weston, and G. Zangari, Phys. Rev. B **64**, 184403 (2001).
[48] E. Goto, N. Hayashi, T. Miyashita, and K. Nakagawa, J. Appl. Phys. **36**, 2951 (1965).
[49] N. Viart, R. S. Hassan, J. Loison, G. Versini, F. Huber, P. Panissod, C. Mény, and G. Pourroy, J. Magn. Magn. Mater. **279**, 21 (2004).
[50] S.-S. Yan, M. Elkawni, D. S. Li, H. Garmestani, J. P. Liu, J. L. Weston, and G. Zangari, J. Appl. Phys. **94**, 4535 (2003).